

Rhodium effects on Pt anode materials in a Direct Alkaline Ethanol fuel cell

Thamyres Fernandes Messa Moreira ^{ab}, Sidney Aquino Neto ^a, Charly Lemoine ^b, Kouakou Boniface Kokoh^b, Cláudia Morais^b, Teko Wilhelmin Napporn^{b*} and Paulo Olivi ^{a*}

^aLaboratório de Eletroquímica e Eletrocatalise Ambiental, Departamento de Química da Faculdade de Filosofia Ciências e Letras de Ribeirão Preto, Universidade de São Paulo, Av. Bandeirantes, 3900, 14040-901 Ribeirão Preto, SP, Brazil,

^bUniversité de Poitiers, IC2MP UMR 7285 CNRS, 4, rue Michel Brunet B27, TSA 51106, 86073 Poitiers Cedex 09, France

1. Optimization of Pt ϕ Br/C catalysts

As pointed out above and before adding Rh co-elements, the preparation of the Pt-based catalysts from the state-of-the-art BAE method was revisited by varying the parameter $\phi = n(\text{KBr})/n(\text{metal (s)})$ from 0 to 6.5. Indeed, it can be observed a color change when adding under vigorous stirring the bromide solution to the precursor metal salt solution composed of the Pt chloride. The bromide effect which consists in replacing the chloride ligands on the metallic ion was followed by UV-vis measurements for 1 h. The Pt0.0/C spectra showed intense absorption band at 262 nm corresponding to ligand-to-metal charge transfer transition for $[\text{PtCl}_6]^{2-}$ ion complex ^{1, 2}. KBr addition leads to a decrease in the intensity of this band, which can be explained by the formation of mixed complex of $[\text{PtCl}_{6-x}\text{Br}_x]^{-2}$ (with $0 < x < 6$) ^{3, 4}. One can also notice the band appearance as shoulder at *ca.* 308 nm indicating a partial substitution of Br⁻ in the structure of the initial complex.

Otherwise, the resulting powders obtained after the reduction step (with NaBH₄) and recovering of the Pt ϕ Br/C samples, XRD and TEM characterizations were undertaken to check the steric effect of the bromide ion on the crystallite size. From Debye's Scherer equation ⁵, the crystallite sizes of the Pt ϕ Br/C samples were estimated, decreasing when the ϕ value increases up to 5.5. Highlighting the (111) plane peaks, Pt5.5Br/C has the smallest size (2.79 nm), and Pt0.0Br/C has the largest one (4.94 nm), which provides sound evidences to the steric

effect playing by the bromide ligand around the metal atom, and stabilizing the particle during the reduction process into Pt5.5Br/C. Nevertheless, in terms of catalytic applications, the metal dispersion on the conducting substrate is also a key factor of enhancing the catalytic activity of the electrode material. Therefore, the Br⁻ behavior on the dispersion of particles was characterized by TEM analysis for Pt0.0Br/C and Pt5.5Br/C. As can be observed on **Figure SI-1**, the images clearly show differences in the shape of the nanoparticles. The Pt0.0Br/C (**Figure SI-1a**) shows dark spots with more agglomeration and less spherical shape particles, while in Figure 1b the Pt5.5Br/C particles are well dispersed on the carbon substrate, with the presence of more particles under spherical shape. Additionally, the mean particle size ($D_{m,p}$) confirms the bromide capping effect on the particle size control. In the case of Pt5.5Br/C the mean particles diameter decreases down to $3.03 \text{ nm} \pm 0.6 \text{ nm}$ in comparison with $4.5 \text{ nm} \pm 0.7$ for Pt0.0Br/C. Compared to the particle size (5.4 nm) of Pt/C catalyst recently prepared by Huang and co-workers⁶ using borohydride reduction process, it is clear that the insertion of Br⁻ has a great effect for controlling the particle growth during the BAE reduction process when the ratio φ is equal to 5.5.

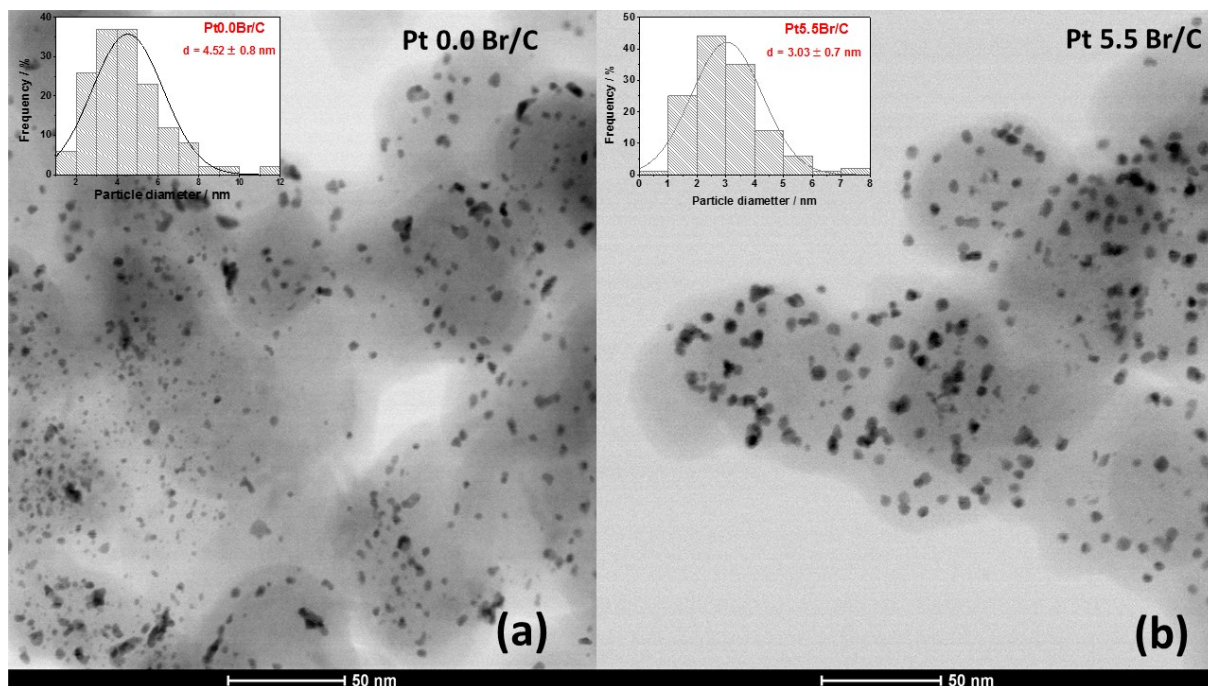


Figure SI-1: TEM images for optimizing the BAE synthetic method on Pt-based electrode materials. **(a)** Pt_{0.0}Br/C and **(b)** Pt_{5.5}Br/C samples in two different amplified regions

The prepared Pt ϕ Br/C samples were then characterized by cyclic voltammetry in a supporting electrolyte (1.0 mol L⁻¹ NaOH) in the potential range of 0.05 - 1.15 V vs. RHE at 10 mV s⁻¹ scan rate. As the specific electrochemical active surface area (SECSA) depends on the current associated with the hydrogen adsorption/desorption region, the recording of the voltammograms of each Pt ϕ Br/C electrode (**Figure SI-2a**) allowed calculating the catalytic activity of the BAE-synthesized samples (considering a 210 $\mu\text{C cm}^{-2}$ coulombic charge for a Pt-H_{ads} monolayer). It can be observed a main change in the hydrogen adsorption/desorption region according to the ϕ parameter. Indeed, the Pt_{0.0}Br/C composition presents a lower peak intensity, which means a lower voltammetric area and subsequently, a smaller amount of available active sites. Conversely, the Pt_{5.5}Br/C composition depicts the highest definition in this characteristic potential domain, which provides another trend of the bromide ligand effect on the electrode surface prepared from the BAE synthetic approach. **Figure SI-2b** shows

that SECSA of the Pt5.5Br/C composition reaches $40 \text{ m}^2 \text{ g}^{-1}$, while that of the Pt0.0Br/C catalyst is $25 \text{ m}^2 \text{ g}^{-1}$, which represents a 37% enhancement.

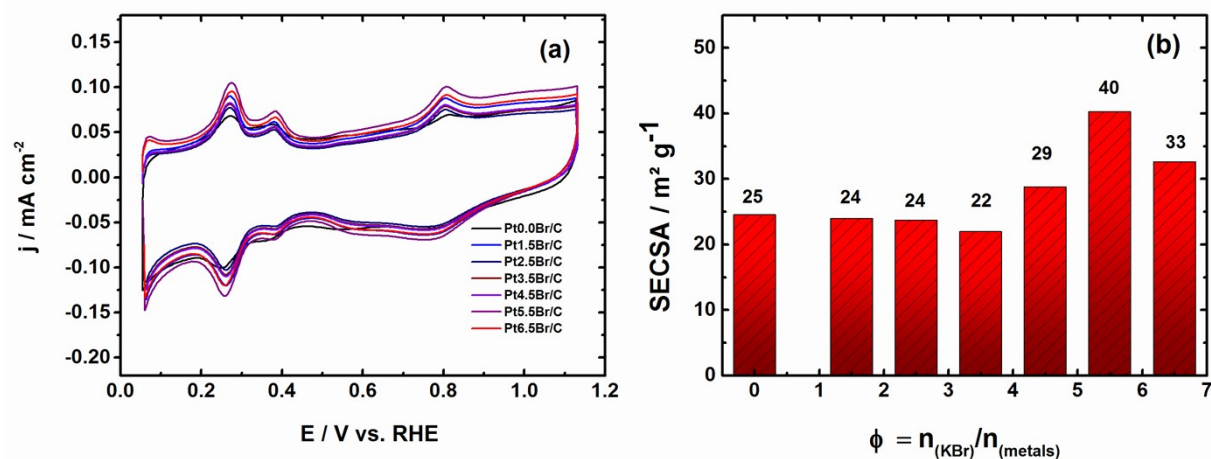


Figure SI-2: (a) Voltammograms of the Pt ϕ Br/C electrodes recorded in NaOH 1 mol L⁻¹ at room temperature and at 10 mV s⁻¹; **(b)** Specific electrochemical active surface area as function of the ϕ parameter for each prepared Pt ϕ Br/C catalyst; evaluation done from **Figure SI-2a**.

From the previous optimization of the BAE protocol probed on Pt-based materials to optimize ϕ at 5.5, different Pt_xRh_y/C catalyst compositions were synthesized under similar conditions and their metal loadings were measured by thermogravimetric analysis (TGA). Typically, the thermogravimetric profiles present similar mass loss behavior as can be seen in **Figure SI-3**. The small weight loss observed at the beginning of the curves (up to 390 °C) is associated with the removal of water adsorbed on the surface. The greatest loss of mass starts at 390 °C (Pt/C) and 423 °C (Pt_xRh_y/C), corresponding to the carbon support combustion, as already reported^{4,7}.

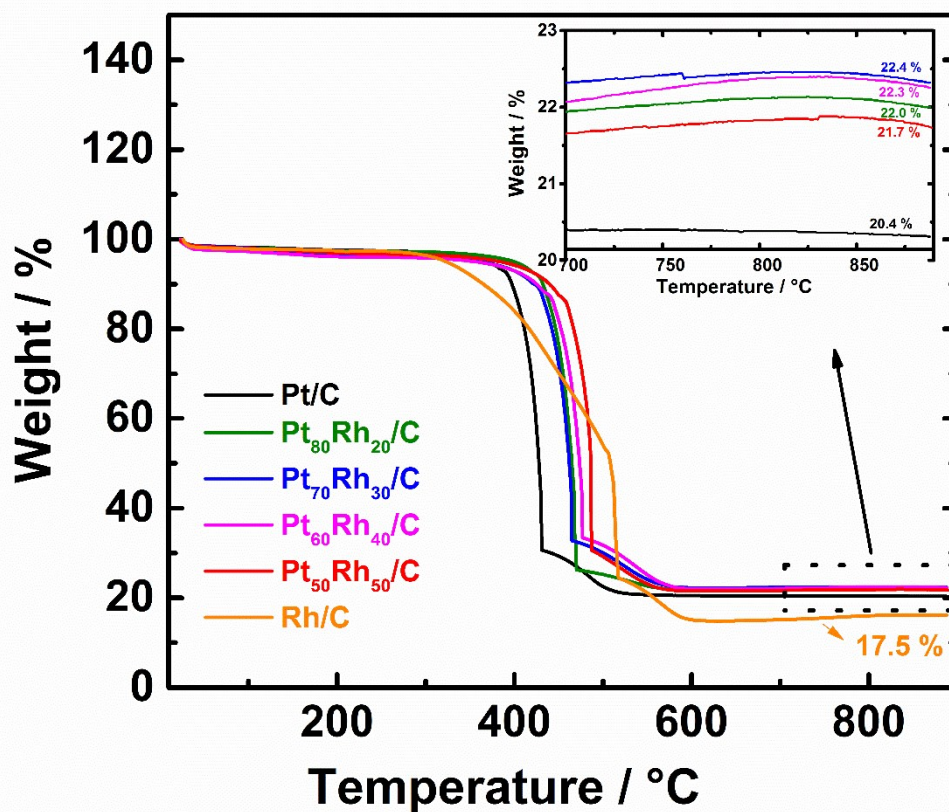


Figure SI-3: TGA curves for the Pt_xRh_y/C nanoparticles in air atmosphere, at 10 °C min⁻¹ linear temperature variation from 25 to 900 °C.

Beyond 600 °C, one an asymptotic trend of the weight is reached, the experimental mass loading of each sample can be deduced. It is comprised between 17.5 (Pt/C) and 22.4% (Pt_xRh_y/C), which is close to the expected 20 wt.% mass loading.

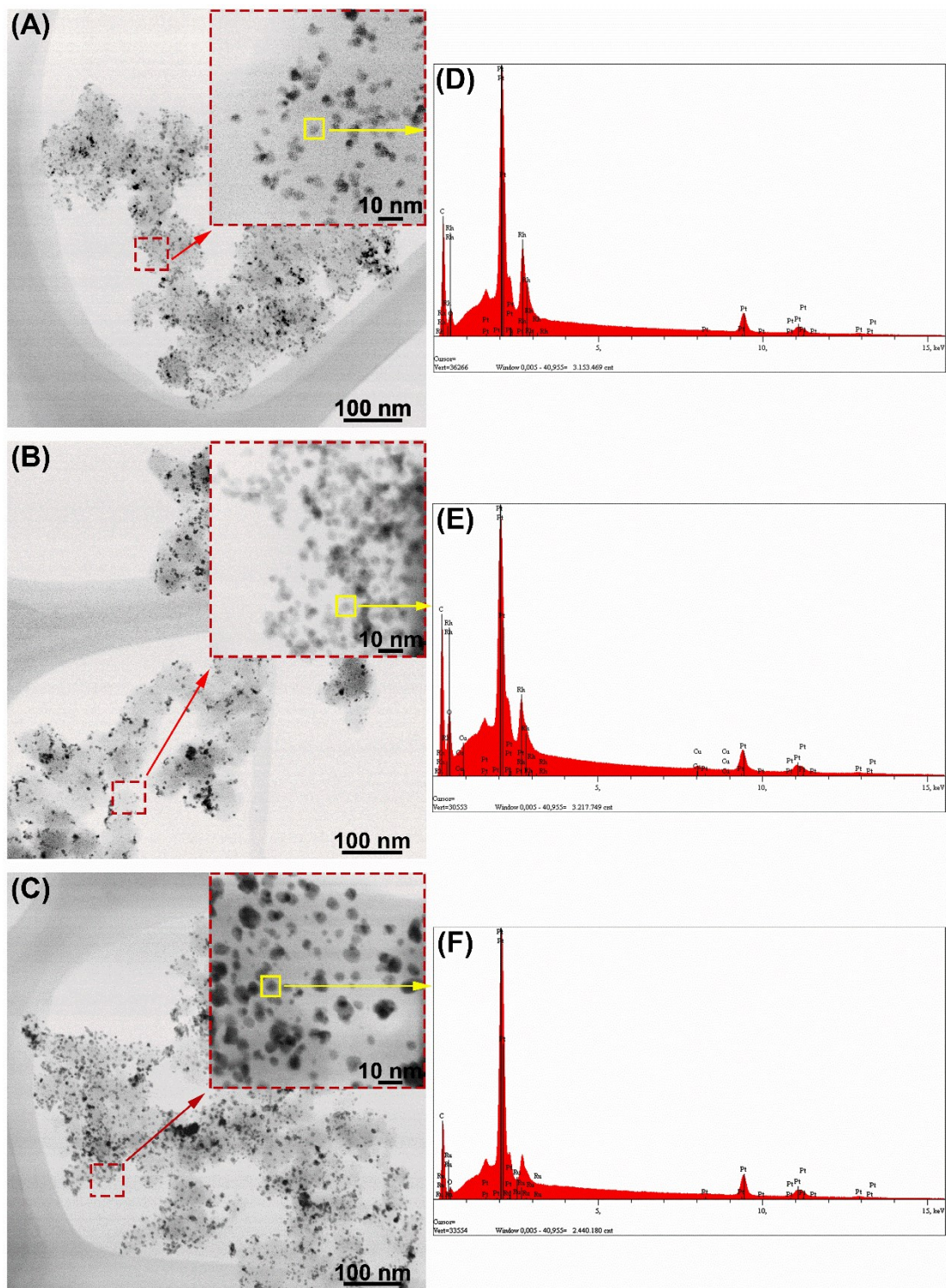


Figure SI-4: (a) TEM images for Pt₆₀Rh₄₀/C material. (d) EDX spectra of Pt₆₀Rh₄₀/C particle; (b) TEM images for Pt₇₀Rh₃₀/C material. (e) EDX spectra of Pt₇₀Rh₃₀/C particle; (c) TEM images for Pt₈₀Rh₂₀/C material. (f) EDX spectra of Pt₈₀Rh₂₀/C particle.

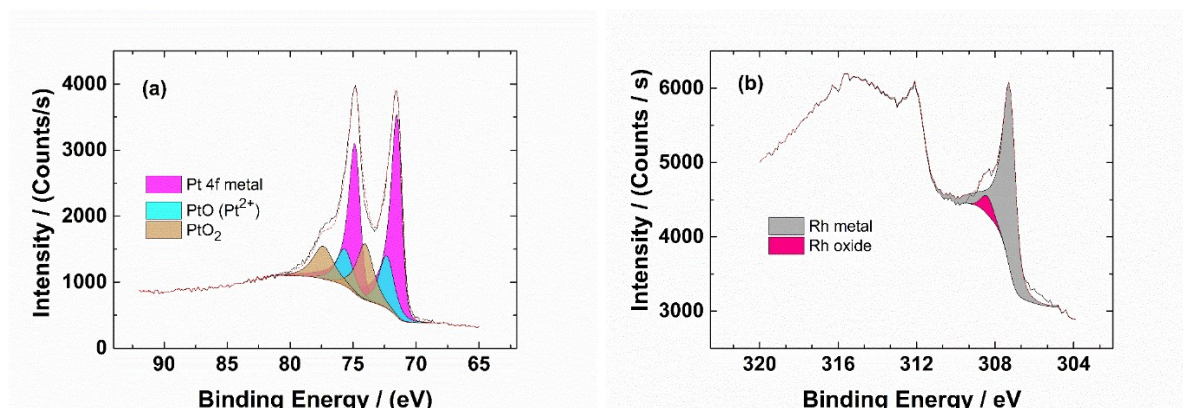


Figure SI-5: X-ray photoelectron spectra of (a) Pt4f and (b) Rh3d in Pt₅₀Rh₅₀/C catalysts.

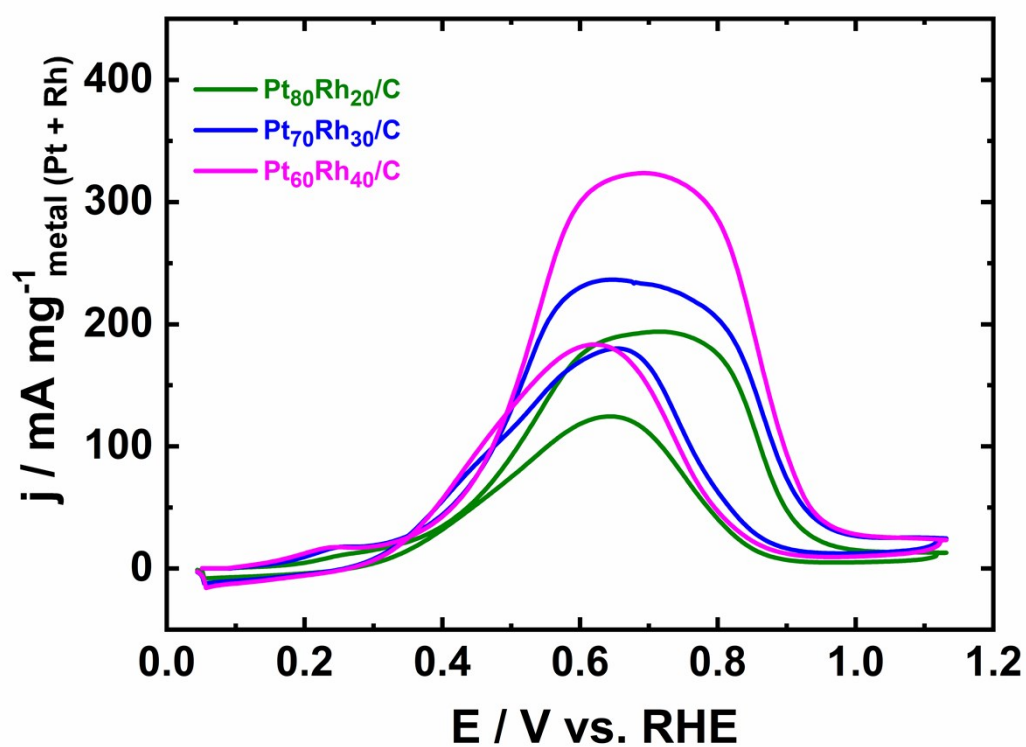


Figure SI-6: Voltammograms (CVs) of Pt and Rh based electrode materials prepared from the revisited BAE route. These CVs were recorded at room temperature, 10 mV s⁻¹ and in 1 mol L⁻¹ NaOH, in the presence of 0.2 mol L⁻¹ ethanol.

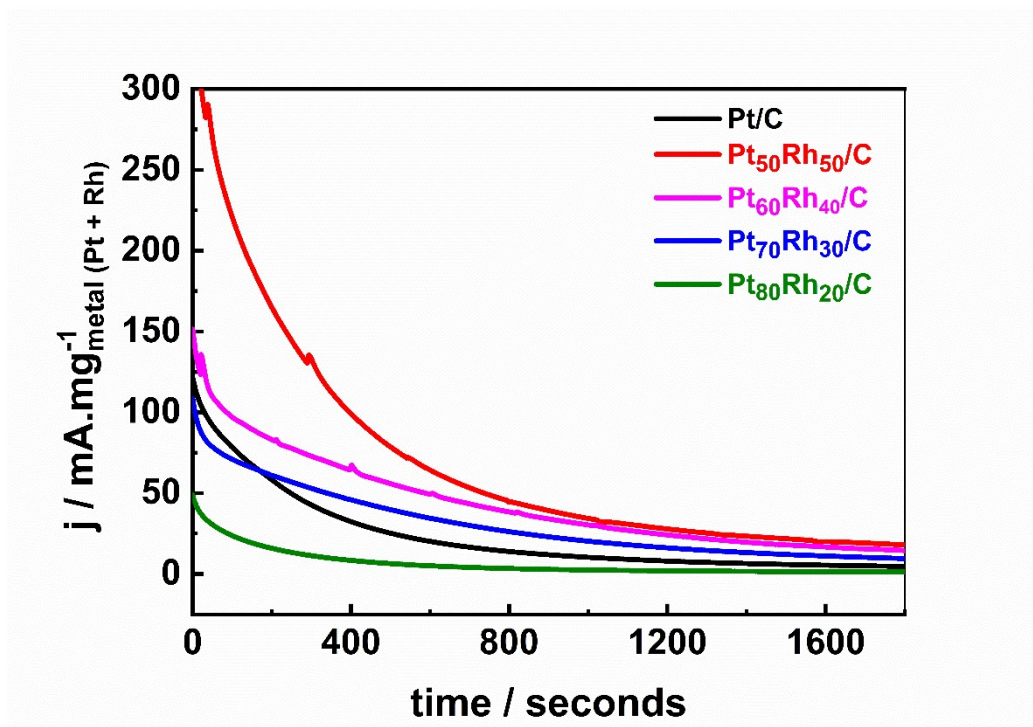


Figure SI-7: Chronoamperometric curves at 0.6 V (vs. RHE) in 0.2 mol L⁻¹ ethanol + 1.0 mol/L NaOH solution during 1800 s.

References

1. M. Mirdamadi-Esfahani, M. Mostafavi, B. Keita, L. Nadjo, P. Kooyman and H. Remita, *Gold Bulletin*, 2010, **43**, 49-56.
2. H. Nagabhushana, R. B. Basavaraj, B. Daruka Prasad, S. C. Sharma, H. B. Premkumar, Udayabhanu and G. R. Vijayakumar, *Journal of Alloys and Compounds*, 2016, **669**, 232-239.
3. Y. Holade, N. Sahin, K. Servat, T. Napporn and K. Kokoh, *Catalysts*, 2015, **5**, 310-348.
4. S. A. Neto, T. F. M. Moreira and P. Olivi, *International Journal of Hydrogen Energy*, 2019, **44**, 8079-8088.
5. I. H. Ko, W. D. Lee, J. Y. Baek, Y. E. Sung and H. I. Lee, *Materials Chemistry and Physics*, 2016, **183**, 11-17.
6. L. Huang, J.-Y. Sun, S.-H. Cao, M. Zhan, Z.-R. Ni, H.-J. Sun, Z. Chen, Z.-Y. Zhou, E. G. Sorte, Y. J. Tong and S.-G. Sun, *ACS Catalysis*, 2016, **6**, 7686-7695.
7. R. G. Da Silva, S. Aquino Neto, K. B. Kokoh and A. R. De Andrade, *Journal of Power Sources*, 2017, **351**, 174-182.